DELPHI 82/1
31 January 1982

CERN/LEPC/82-8
LEPC/I6
25.3.1982

DELPHI

A DETECTOR WITH LEPTON, PHOTON AND HADRON IDENTIFICATION

Letter of intent for an experimental program at LEP

DELPHI COLLABORATION

GROUP	CONTACTMAN
Collège de France	M. Crozon
Ecole Polytechnique	M. Urban
Orsay	F. Richard
Paris – LPNHE	M. Baubillier
Saclay	G. Smadja
Strasbourg	A. Degré
Karlsruhe	J. Engler
Wuppertal	J. Drees
Oxford	G. Myatt
Rutherford	W. Venus
Athens – Nat. Tech. Univ.	T. Filippas
Athens	L. Resvanis
NIKHEF – Amsterdam	F. Udo
INFN – Bologna	L. Monari
INFN – Genoa	M. Bozzo
INFN – Milan	A. Pullia
INFN – Padua	L. Ventura
INFN – Rome – Sanità	C. Bosio
Bergen	E. Lillestøl
Oslo	T. Buran
Cracow	K. Rybicki
Lund	G. Jarlskog
Stockholm	G. Ekspong
Uppsala	S. Kullander
CERN	J.V. Allaby

1. INTRODUCTION

This letter expresses the intent of physicists from 25 European laboratories to explore to the fullest extent the exciting fields of physics which will be opened up by the new CERN e^+e^- collider. The Collaboration has been formed around a common interest in specific physics subjects and a common intention to build a high-performance detector. Indeed we believe that LEP physics should not be limited to the gross features of Z^0 physics, but should extend to the detailed analysis of the final states and of possible unexpected effects. As a consequence we propose to build the detector, shown schematically in Fig. 1, which is based on a solenoidal magnetic field and is further characterized by:

a) *hadron and lepton identification over ~ 90% of the full solid angle;*
b) *fine spatial granularity of all the components;*
c) *three-dimensional information on every track and energy deposition (rather than stereo views).*

Particle identification [point (a)] is achieved by combining conventional methods (4π coverage with electromagnetic and hadronic calorimeters and muon chambers) with ionization measurements in the Time Projection Chamber (TPC) and with velocity measurements based on the Ring-Imaging Cherenkov (RICH) counters, a technique under development within our Collaboration. This latter technique is particularly appropriate in the forward direction ($\theta \lesssim 35°$) where good ionization measurements are difficult to achieve. The choice of the TPC (recently shown to be a successful track detector by the LBL group [1]) and of the other components of our detector, many of which are based on drift measurements, guarantees the fine granularity [point (b)] and the three-dimensional nature of the collected information [point (c)].

In the definition of an experimental program, two related and complementary aspects enter: the choice of the physics questions, and the selection of the experimental techniques most suitable to answering such questions. In the case of LEP, both choices are very challenging because of the rich field of physics which can now be foreseen and because of the long lead-time. For the physics, we work under the assumption that the standard model of the electroweak theory is correct and, because of the rates, we focus mainly on the Z^0 peak. The scenario may well be more complicated, but we believe that optimizing the detector to check the standard model thoroughly and accurately is also the best way to prepare oneself for surprises. Section 2 contains the list of problems we want to address, and focuses on the properties of our detector that are specially suited to tackle these problems.

As far as the experimental techniques are concerned, the proposed detector contains novel features. At present we are building prototypes of these novel components, and we consider their successful test as a necessary condition for their inclusion in the final proposal. Section 3 presents in detail the detector, describes the prototype work already done or under way and, where appropriate, gives the alternative solutions we are working on. We intend to have the detector working from day one of LEP. Since we are convinced that these large detectors will evolve during their long lifetime, possible financing or technical delays could be coped with by recognizing that certain components are crucial for the basic physics program while others could become operational later. For the same reason, we foresee some possible lines of development based on the addition of more and more advanced components.

Section 4 contains a first cost estimate and an indication of the sharing of responsibilities among the groups.

2. PHYSICS AIMS

In this section we spell out our main physics goals and the main properties of the detector shown in Fig. 1 which make it suitable for tackling these problems. Quantitative arguments backing up these short qualitative statements are contained in internal notes of the Collaboration and collected in the report DELPHI 82/2.

2.1 Basic Z^0 physics

This physics is an essential part of our experimental program and will also allow the understanding of the various components of the detector. Even with the lower limit of the luminosity given by E. Picasso [2], LEP will provide 1.5 million Z^0 events in one calendar year (2500 h).

a) The position, width, and cross-section of the Z^0 peak will be measured almost on-line based on a good ($\pm 3\%$) luminosity monitor using Bhabha scattering. The charges and momenta of lepton pairs will be measured down to small angles ($\theta \gtrsim 15°$) in order to increase the sensitivity to charge asymmetries (at the Z^0 peak the error will be $\pm 1\%$). The polarization of $\tau^+\tau^-$ pairs will be determined from the spectra of the decay π's and ρ's, as suggested by some of us [3]. Since this polarization and many other asymmetry effects are much larger with polarized beams, we consider beam polarization an important tool in the energy range of LEP Phase 1. These measurements already constitute precise checks of the standard model, and test for possible large couplings of the Z^0 to new leptons, new quarks, etc. For example, the number of neutrinos could prove to be measurable within ± 0.3.

b) New sequential leptons and quarks will be sought more directly by identifying high-energy electrons and muons and measuring global jet properties, (e.g. spherocity, energy flow). The detection of missing energy is a valuable tool in new heavy-flavour searches.

c) We intend to hunt for signs of the relatively unexpected, such as free quarks and the effects of supersymmetries (e.g. scalar leptons decaying into ordinary leptons plus non-interacting photinos and goldstinos carrying large missing transverse momentum), effects of quark and lepton substructure (e.g. $\mu^* \rightarrow \mu\gamma$ decays), etc.

For this basic physics program, from "day one" the detector will separate electrons and muons from hadrons, detect neutral energy flow, measure the charges of 50 GeV/c particles for angles larger than $\sim 15°$, and be sensitive to less than minimum ionization. Missing momenta will be detected with the help of the $\sim 4\pi$ hadron calorimeter.

2.2 Jet studies

At the present e^+e^- colliders, two-jet and three-jet events have been extensively studied. However, LEP will increase the available energy range and produce very large samples of events with two and three energetic jets, with which we are interested in completing the study of parton fragmentation functions. The rarer four-jet events will give an important contribution to quark and gluon physics. We want to identify hadrons inside the jets so as to fully exploit the many events that can be collected at the Z^0 peak and study strong and weak interaction effects.

a) Semileptonic decays observed in $b\bar{b}$ and $t\bar{t}$ jets provide a very useful method for understanding the weak decay cascades of these heavy flavours and measuring the generalized Cabibbo angles. Monte Carlo studies show that the spherocity or thrust of the event, combined with the measurement of the transverse and longitudinal momenta of electrons, muons, and kaons relative to the jet axis, will allow the tagging of the produced quark pair. Electron/muon/pion/kaon separation is needed for such a program.

b) We are interested in separating gluon jets from quark jets. This can be attempted by identifying the electrons and the hadrons (in particular the baryons) of momenta smaller than about 10 GeV, and recognizing quark jets as discussed under point (a). Well-identified four-jet events are expected to be quite common at LEP. We are interested in them because their angular distribution contains information on the three-gluon coupling. Within the Lund model the three-gluon coupling gives also rise to particular effects in the fragmentation to kaons and protons, e.g. a depletion in the relative number of low-momentum kaons and a small increase in the number of leading baryons.

c) Heavy flavours will be abundantly produced on the Z^0 peak. Since 90% of the particles from a beauty-meson decay have momenta below 10 GeV/c, good particle identification and π^0reconstruction are needed in this energy range. With identification and $\Delta p/p^2 = 0.3\%\ \mathrm{GeV}^{-1}$ around 10 GeV/c the mass resolution is better than 2%. Reconstructed π^0's will not alter this mass resolution provided that $\sigma(E)/E \lesssim 15\%/\sqrt{E}$. The combinatorial background will be effectively reduced with a high-resolution vertex detector which identifies secondary vertices from short-lived particles. A silicon detector which can give point accuracy $\lesssim 10\ \mu m$ and could be placed at a few centimetres from the vacuum pipe has been developed within our Collaboration.

d) The weak couplings of the Z^0 to the quarks can be obtained by measuring the charge asymmetries of identified $q\bar{q}$ pairs. The knowledge of the charges of the outgoing leptons and the measured spherocity of the event can identify $t\bar{t}$ and $b\bar{b}$ events. Quark identification can be backed up by the information of the vertex detector. With the expected rate, the charge asymmetry will be measured with a statistical error smaller than 1%, which provides a precise test of the theory. Identification in the forward arms of leading charged kaons (momenta larger than 10 GeV) will allow the statistical tagging of $s\bar{s}$ events. It must be noted that, for measuring asymmetries, the forward events with $\theta \leq 30°$ are as effective as the events in the range $45° < \theta < 135°$.

For this chapter of physics, electron, muon, and hadron identification in a jet is a necessary tool. Most of the experiments need good hadron identification below $z = 0.2$ (momenta smaller than ~ 10 GeV) and $\Delta p/p^2 \simeq 0.3\%$ GeV^{-1} around 10 GeV/c. In particular, the clean kaon/proton separation achievable with the RICH counters, and not with ionization measurements, is essential. Electrons will be distinguished from pions with rejection factors larger than 10^3; this will be obtained in the angular range $40° \leq \theta \leq 140°$ by combining the information of the electromagnetic calorimeter with ionization measurements. The granularity of the electromagnetic calorimeter ($\lesssim$ 20 mrad) is such as to manage the γ-π overlap problem. The tagging of quark jets for asymmetry studies (in particular of $s\bar{s}$ jets) requires K identification at momenta larger than 10 GeV, which will be done by the RICH counters in the forward cones. Beam polarization is highly desirable for asymmetry measurements.

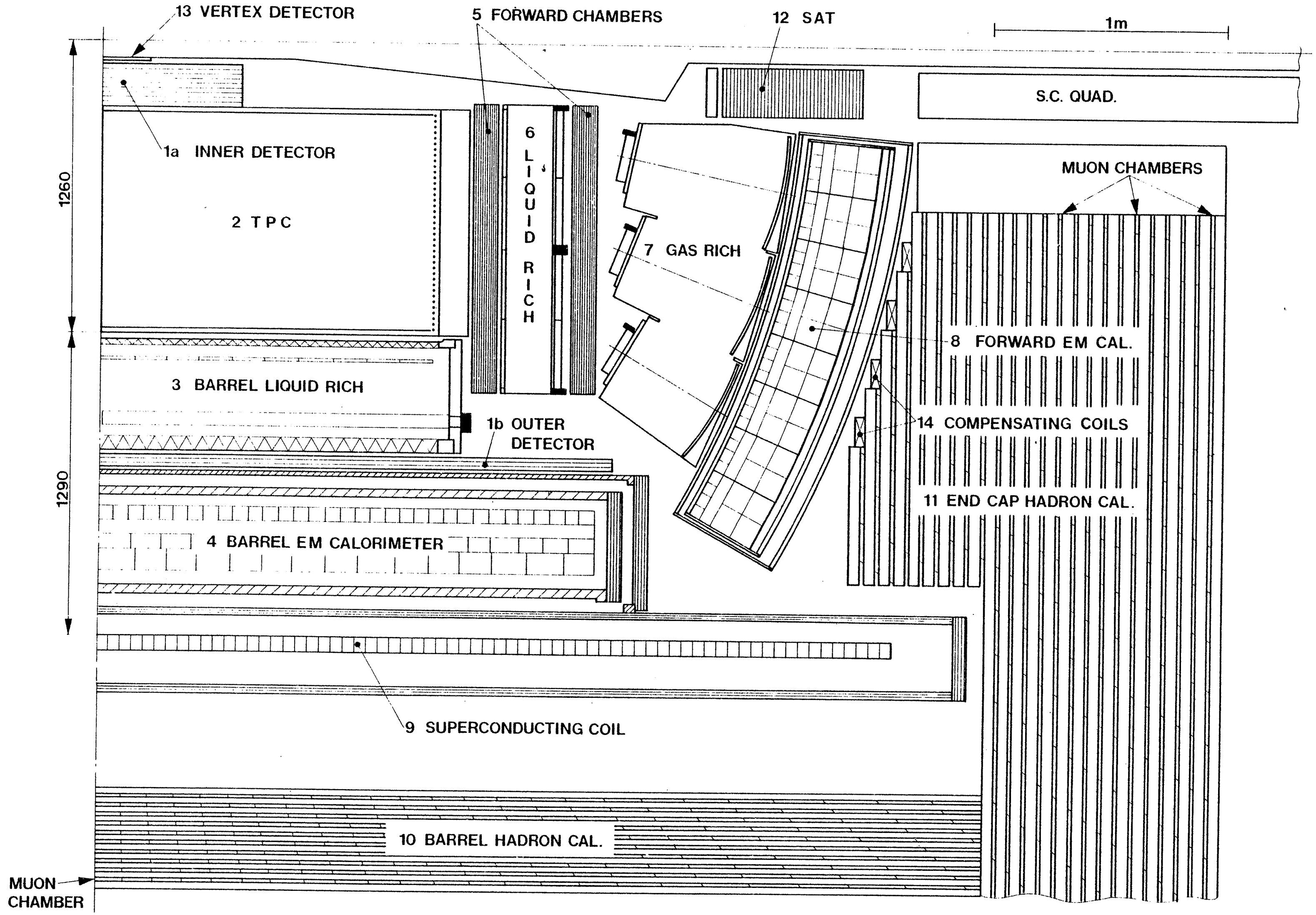

Fig. 1 **1a.** The inner detector is a drift chamber giving 12 points on each track. **1b.** The outer detector is formed of three layers of drift tubes and, together with the inner detector, is used in the trigger. **2.** The 1 atm TPC gives three-dimensional space points and separates pions and electrons up to $\sim$ 8 GeV/c by ionization measurements. **3.** The cryogenic barrel liquid RICH counter identifies kaons up to $\sim$ 8 GeV/c. The radiator, the photon detector and the honeycomb structure of the walls are indicated. **4.** The tower structure of the liquid-argon calorimeter within its cryostat is shown. **5.** Forward drift chambers. **6.** The warm liquid RICH counter gives π/K separation up to $\sim$ 5 GeV/c. **7.** The photons produced in the gas RICH counter are focused by spherical mirrors, allowing π/K separation up to $\sim$ 35 GeV/c. **8.** The tower structure of the forward liquid-argon calorimeter is similar to that of the barrel calorimeter. **9.** The superconducting coil, of 2.55 m radius **10. + 11.** The tower structure of the hadron calorimeter embedded in the iron return yoke is shown. Some planes are instrumented with 4 cm cathode strips for muon identification. **12.** Small-angle tagger. **13.** Location of the silicon microstrip vertex detector. **14.** Warm compensating coils.

2.3 Scalar bosons

LEP offers unique possibilities to search for neutral and charged bosons (Higgs bosons, technipions) and scalar quarks or leptons. Our experimental program puts a major emphasis on such a line of research. It includes possibilities to study both the production and the decay modes of such particles, should they exist within reach of LEP. The predicted similarity of elementary Higgs bosons and technipions requires the fullest possible information on the hadronic and leptonic content of the decay products of the few precious events we may collect for understanding the nature of any peak in the missing-mass spectrum. The same requirement is true for scalar quarks and leptons, which will be abundantly produced, if they exist in the LEP range.

a) With LEP tuned to the Z^0 peak, the best way to search for neutral Higgs is through the reaction $e^+ + e^- \rightarrow Z^0 \rightarrow H^0 + \ell^+ + \ell^-$, where the final-state leptons have to be well measured. The tracking detector together with the e.m. calorimeter (with resolution $\sim 0.12/\sqrt{E}$) will serve this purpose for e^+e^-pairs. The r.m.s. mass resolution varies roughly as $m_H^{-1/2}$ and will be about 2 GeV for $m_H = 20$ GeV. During the first year of running, the mass range from a few GeV to a few tens of GeV can be covered, the upper end being limited by rate [4] and background. The e.m. calorimeter alone will be used to search for the monochromatic gamma-ray in the rarer reaction $Z^0 \rightarrow H^0 + \gamma$.

b) The reaction $e^+ + e^- \rightarrow Z^0 \rightarrow H^0 + \nu + \bar{\nu}$ is at least six times more probable than the reaction with e^+e^- in the final state, and one can expect about one hundred events per year for $m_H \simeq 20$ GeV. The signature is a large missing transverse momentum requiring a 4π fine-grain calorimeter to measure the energy and direction of neutral hadrons and reduce the background events. Monte Carlo calculations show that we will obtain mass resolutions of the order of $\Delta m_H/m_H \simeq 0.15$ with a hadronic calorimeter of moderate energy resolution. This technique also gives access to channels with $\mu^+\mu^-$ in the final state.

c) Fundamental charged scalar particles, if they exist, will be detectable in the decay $Z^0 \rightarrow H^+ + H^-$ [3] albeit with a very low rate. If they couple like neutral Higgs, their signature will be the decay into heavy flavours $H^\pm \rightarrow \tau^\pm \nu_\tau$, $H^- \rightarrow \bar{c}s$ and $\bar{t}b$. The hadronic channels give the possibility to reconstruct the mass with an error $\Delta m_H/m_H \simeq 0.1$. Flavour tagging, and hence particle identification, will once again be a powerful tool.

This part of the program requires the same detector properties necessary for the detailed study of jets already discussed in subsection 2.2, with emphasis on the requirement that electrons of $\sim$ 40 GeV will be measured with errors < 1 GeV, whereas it is enough to detect neutral hadrons with moderate energy resolution (e.g. $0.8/\sqrt{E}$) and angular resolution of the order of 2°.

2.4 Neutrino counting and other topics requiring photon detection

A direct measurement of the number of neutrinos can be obtained from the process $e^+ + e^- \rightarrow Z^0 + \gamma \rightarrow \nu + \bar{\nu} + \gamma$ at an energy somewhat above the Z^0. As shown in Ref. 5, this leads to a peak in the photon energy distribution which makes this process distinguishable from the background of bremsstrahlung photons.

The experiment will be done by detecting single photons in the energy range 2–50 GeV for angles $\theta > 5°$, and by checking that no other particle was emitted within the large solid angle covered by our detector.

Photons of larger energies have to be detected over a large fraction of the solid angle to study the reaction $e^+ + e^- \rightarrow \gamma + \gamma$, which is sensitive to the structure of the virtual electron down to distances of 10^{-17} cm.

2.5 Top quark physics

If the mass of the top quark is larger than about 20 GeV, LEP may be the only machine to produce it. If the mass is large, weak decays will dominate and give flavour cascades with the production of leptons, short-lived particles and, eventually, kaons. Their identification will be essential in order to understand the decay properties of the cascading quarks. Charged Higgs and technipions, if they exist with mass smaller than the top mass, will be the main decay channel ($t \rightarrow H^+b$). *Again, the final state will contain kaons of energies smaller than about 10 GeV, which will be identified over $\sim$ 90% of the full solid angle.*

For top quarks lighter than 30 GeV, we believe it will be possible, on the Z^0 peak, to estimate the mass accurately enough to narrow down effectively the search for the toponium states. Neutral Higgs and technipions will be looked for in the $H^0 + \gamma$ and $P^0 + \gamma$ decays of the toponium states using the electromagnetic calorimeter. A cascade to short-lived particles and many kaons, accompanied by a monochromatic gamma, will provide a signature for such decays.

2.6 Two-photon physics

We are primarily interested in the measurement of the photon structure functions. In order to investigate the strong interaction corrections to the point-like (Born) approximation of these functions, we shall observe deep inelastic e-γ scattering over a wide range of momentum transfers ($1 \leq Q^2 \lesssim 50$ GeV^2) by tagging the scattered electron both in an electromagnetic shower detector located in front of the low-beta quadrupoles and in the end-cap calorimeter. The good momentum resolution in a large angular range extending towards forward directions (we aim at $15° \leq \theta \leq 165°$) will allow the determination of the invariant mass W of the recoiling hadronic system. We expect a number of hadronic events satisfying $Q^2 \geq 3\,(\mathrm{GeV/c})^2$ and $W^2 \geq 3$ GeV^2 of the order of 100 per pb^{-1} of integrated luminosity.

3. THE DETECTOR

3.1 Generalities

In the detector shown schematically in Fig. 1 the superconducting coil provides a 1.2 T field of good uniformity, as required by the various detectors which drift electrons along the magnetic field. The Time Projection Chamber (TPC) is the heart of the track detector. Its superior pattern recognition properties and the tridimensional space-point information are needed to reconstruct events with complex topology. Our TPC is only slightly larger than the Berkeley one, but the accuracy in determining momenta larger than ~ 5 GeV/c is improved by the outer detector, made of three layers of drift tubes placed 1.8 m away from the interaction point. In our opinion, energy loss measurements alone will never give adequate π/K and in particular K/p separation. As a consequence, we plan to run the TPC at atmospheric pressure, which greatly simplifies the construction, and count on the $\Delta E/\Delta x$ measurements (σ = 5.5%) mainly to separate electrons from pions at momenta smaller than ~ 8 GeV/c. (The possibility of having some overpressure is at present left open.) All the performance data concerning the TPC are based on results of tests performed for us by the Berkeley group on their TPC run at 1 atm [6].

The inner detector provides good position accuracy (less than 100 μm per wire) for vertex extrapolation and, together with the outer detector, is used for triggering on charged particles. A vertex detector based on semiconductor techniques to improve the vertex resolution is under study and will be implemented in the final proposal. The two forward chambers provide trigger information and good momentum measurements in the end-cap region.

Charged hadron identification is based upon the three Ring Imaging Cherenkov (RICH) counters, which give safe separation also around 1 GeV, where π's and K's are confused by $\Delta E/\Delta x$ measurements. As required by our physics aims, the cryogenic barrel RICH counter will separate π's from K's up to ~ 8 GeV/c, whilst for angles smaller than 35° the combination of a gas and a warm liquid RICH counters covering the forward cone separates π's from K's up to ~ 35 GeV/c. Furthermore, the forward RICH counters improve the momentum measurement in the end-cap region. The positioning and mounting of the RICH counters allows the possibility of a gradual implementation if necessary.

The barrel electromagnetic calorimeter is placed inside the coil to minimize the thickness of material in front of it. Since it must measure, with good accuracy, energies as large as 90 GeV (LEP 2) in an environment which does not provide many calibration lines, we have chosen a detector with a *linear* response. Figure 1 is based on a liquid-argon solution, but we are also working on a new promising development, the High-density Projection Chamber (HPC) [7]. Such a high-granularity device would allow efficient π^0 reconstruction, would be a unique tool for identifying high-energy π^0's up to 20 GeV, and would provide better e/π separation than would the liquid-argon calorimeter. The end-cap electromagnetic calorimeter is a liquid-argon counter with towers in projective geometry. In both argon calorimeters, strips interleaved with the towers cover about 1°.

The hadron calorimeter is made by laminating the return yoke of the magnet and inserting active elements in the form of towers covering about 2° × 2°. The active elements are plastic tubes working in limited streamer mode, and the readout is made on pads in projective geometry. Planes of streamer tubes act as muon chambers. On each plane, three stereo coordinates are read with strips which, for the first round of experiments, will be connected so as to be 4 cm wide. The system allows the later implementation of external muon chambers.

In the following sections the components of the detector are briefly presented. More details are contained in internal notes of the Collaboration and are summarized in the report DELPHI 82/3.

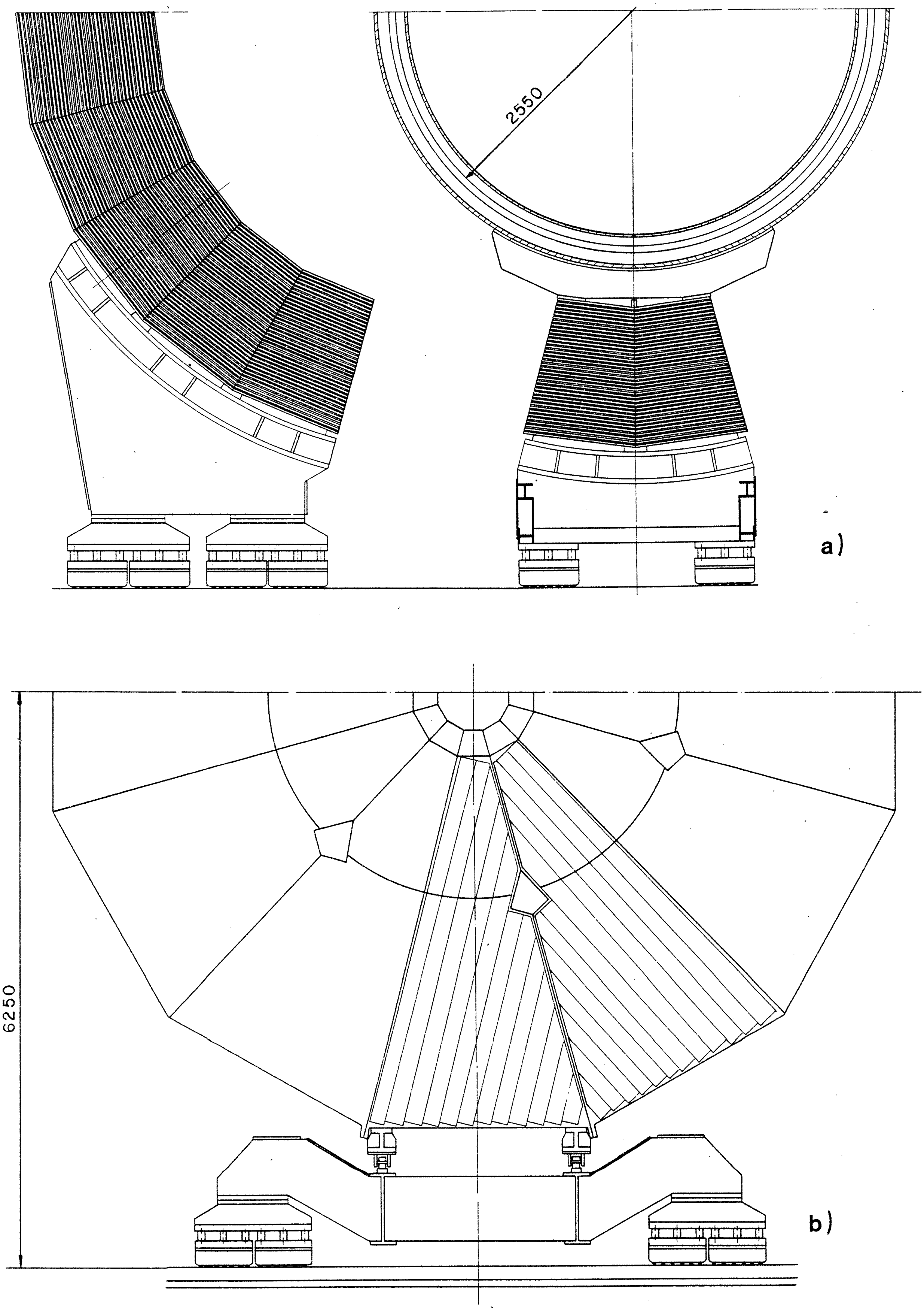

Fig. 2(a) The two lower stacks of the return yoke are part of the barrel hadron calorimeter, support the coil cryostat and the detectors inside it, and move independently along the same rails used to displace the two shells of the return yoke (11 stacks each). **(b)** The double support system is such that each magnet pole, formed by 12 sectors, can be rolled out along the beam axis and also transversally to it to leave access to the internal parts of the detector. The streamer tubes of the hadron calorimeter are arranged as shown in the figure. The holes in the pole are used for cables and cryogenic connections.

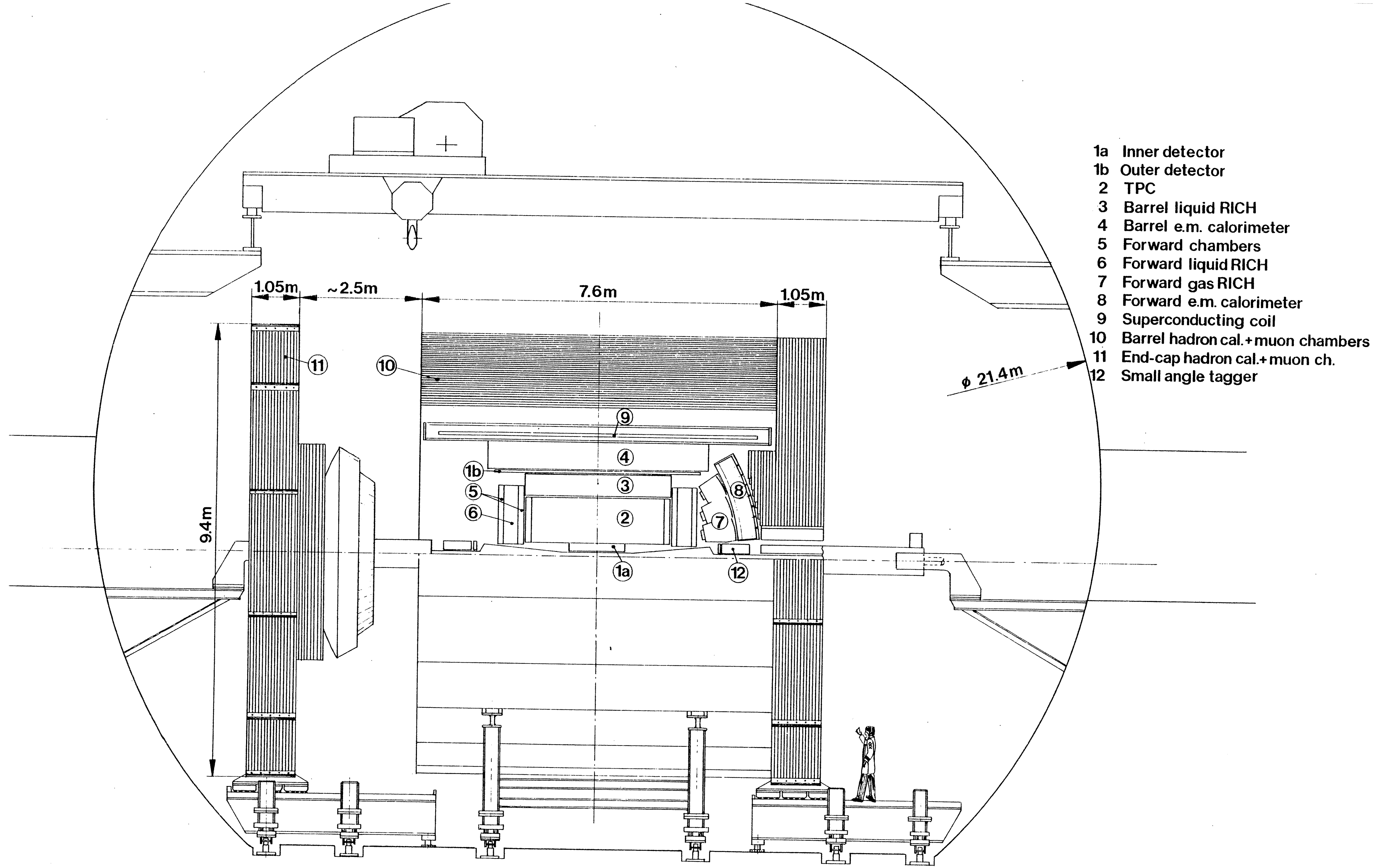

Fig. 3 The experimental hall is wide enough to retract the poles, the forward eléctromagnetic calorimeter and the gas counters mounted on them, when the experiment is sitting on the interaction point.

3.2 The magnet

The magnet consists of a superconducting solenoid of 2.55 m radius and 6.8 m length producing a field of 1.2 T, and of a calorimetrized 2400 ton iron return yoke. This yoke is made of a central cylindrical part, the "barrel", and two "end-caps". In designing the magnet, the safety aspect, the ease of operation with minimum interference with LEP running and the parameters and constraints of the experimental area as presented at the Villars-sur-Ollon meeting have been taken into account. The only exception is the crane capacity, which should be increased to about 60 tons. The extra cost would be more than compensated by savings in the machining of the return yoke.

The central part of the return yoke is formed by 24 equal, longitudinal modules made by stacks of 2.5 cm thick iron plates separated by 1.5 cm for calorimetrization. The two bottom modules of the barrel are used for supporting the coil cryostat, which itself supports the various detectors located inside it (Fig. 2a). The other 22 modules of the barrel are assembled in two arches which are mounted on separate supports rolling on rails perpendicular to the LEP beam. In this way it is possible to open the barrel to provide access to the region surrounding the cryostat.

The two end-caps are each formed by 12 equal, sector shaped, modules made of 5 cm thick iron plates spaced by 1.5 cm. Each end-cap (Fig. 2b) can be displaced longitudinally, with respect to the LEP beam, by about 2.5 m to permit access to the inside detectors; for that purpose the end-caps can roll on small platforms (Fig. 3). The opening-up of the apparatus is designed to be a rapid and straightforward operation, involving no displacement of LEP elements nor any need to interrupt the vacuum. For major interventions, the whole detector and associated electronics will roll out of the LEP interaction region.

The coil is wound with a cryogenically stable hollow cable cooled by a forced flow of liquid He at 4.5 K. The current in the superconducting coil is 10 kA at the maximum field (1.2 T). This current was chosen as a compromise between the requirement of low refrigeration charge for the current leads and a need for a not too large inductance for the coil. The inductance is 1.7 H and the stored energy is $\sim$ 80 MJ. The nominal cryogenic losses are 500 W.

The design of the end-caps includes 2×4 small (conventional) compensating coils (Fig. 1). These coils, which consume about 0.5 MW, permit an increase in the useful volume in the forward regions. In addition they provide flexibility in that their current can be adjusted to achieve the desired field uniformity. Calculations made using an extended version of the computer program "Poisson", have shown that the radial component of the field integral in the axial direction over the TPC drift volume is always less than 50 G · m and in the region of the electromagnetic calorimeter the radial field components are below the level needed for the operation of the HPC (150 G · m).

The detailed design of the magnet is now being developed by the Genoa group and a specialized and experienced firm [8], in consultation with M. Morpurgo, who is the CERN linkman for this superconducting coil.

3.3 The track detector

The track detector comprises the TPC, the inner and outer detectors, and the forward chambers.

We have chosen a TPC as central detector because of its intrinsic power of pattern recognition. At variance with the LBL 10 atm TPC, ours operates at 1 atm to reduce the serious space-charge problem which is proportional to the pressure, to reduce multiple scattering and γ-conversion, and to obtain a faster response (better two-track separation) and a simpler construction (e.g. 20 kV field-cage voltage versus 200 kV at 10 atm). We lose some momentum resolution ($\Delta p/p^2 = 0.5\%$ versus 0.4% and 0.3% at 4 and 10 atm, respectively) and $\Delta E/\Delta x$ resolution [$\sigma(\Delta E/\Delta x) = 5.5\%$ versus 3.6% and 2.7% at 4 and 10 atm, respectively]. This $\Delta E/\Delta x$ resolution is sufficient to separate electrons from pions up to about 8 GeV at the conventional level of 3 standard deviations (Fig. 5a). By combining it with the separation provided by the barrel RICH counter (also plotted in Fig. 5a) and with the hadron-electron separation given by the electromagnetic calorimeter (most effective at higher energies, as shown in the same figure), we shall be able to detect 0.3–50 GeV electrons with 90% efficiency whilst achieving over-all rejection factors for hadrons larger than 10^3, as required by our physics aims. The TPC parameters are listed in Table 1. The values for the z and $\Delta E/\Delta x$ resolutions come from the tests done for our Collaboration by the Berkeley group. The ($r\phi$) resolution is an extrapolation to B = 1.2 T using the results obtained during these tests [6]. At present we foresee the installation of an electrostatic screen in front of the end-plates to reduce the effect of the ion current produced by the proportional wires.

Within our Collaboration, a full-scale TPC sector is under construction and will be tested early in 1982 with 250 electronic channels. A large field-cage and a pressure vessel ($L = \varnothing = 1.5$ m) are being built and will be ready in July 1982. Laser calibration has been tested in a large drift chamber at the ISR and is pursued intensively. Two magnets ($\varnothing = 20$ cm, $B \leq 1.5$ T, $L \leq 1.5$ m) have been commissioned, and various tests on longitudinal and transverse diffusion, on pad structures, and on electronics have started.

Table 1

TPC parameters

Pressure = 1 atm	Gas: Argon + 20% CH_4
L = 2 × 1.45 m	$\sigma(r\phi) = 250\,\mu m$
R = 0.3–1.26 m	$\sigma(z) \leq 1$ mm
$\int B_r\, dz \leq 50$ G·m at 1.2 T	$\sigma(\Delta E/\Delta x) = 5.5\%$
No. $(\Delta E/dx)$ samples = 212	Two-track separation $\leq 2 \times 2\ cm^2$
No. of radial points = 16	Number of sectors = 2 × 6

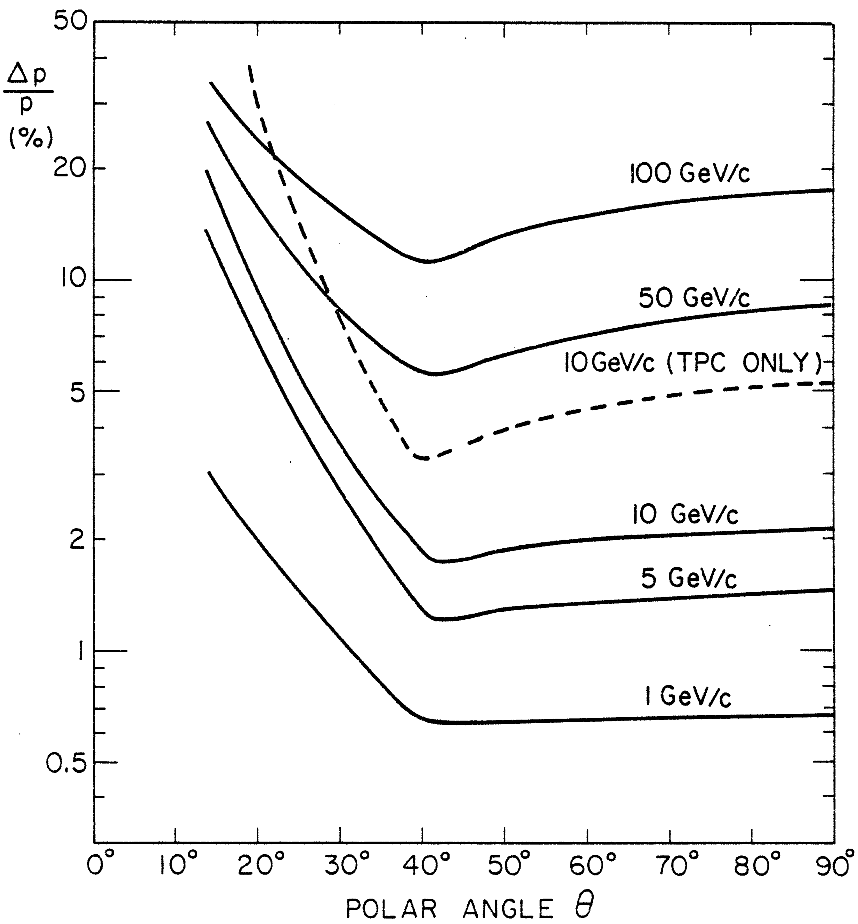

Fig. 4 The momentum resolution of the system of track detectors (inner detector, TPC, outer detector and forward chambers) is computed taking into account measurement errors and multiple scattering. Even at 100 GeV (LEP2) and for angles $\theta \geq 15°$ the charge of a single track will be determined unambiguously (probability of wrong-sign assignment $< 10^{-3}$).

The inner detector has to a) provide trigger information in ($r\phi$) and z directions (granularity $\sim 1°$); b) have a space resolution better than 100 μm per point to extrapolate accurately to the vertex; c) separate tracks at < 1 mm within jets. The chamber contains 1800 wires and is split into two parts to optimize for the particle separation and the trigger requirements separately. It contains a section measuring 12 points on the track by drifting the electrons alternatively to the right and the left, giving the required track separation, and a section containing three layers of closely spaced anode and field wires enclosed in Styrofoam cylinders carrying cathode strips for z-coordinate readout. Present prototype work centres on the use of $Ar\text{-}CO_2$ gas in various geometries.

The outer detector is based on modules of 24 square drift tubes grouped in three layers, each layer being shifted with respect to the previous one. The 3100 tubes are 2×2 cm^2 in cross-section and 2.2 m in length. The transverse position ($r\phi$) of a track is determined by the drift time and the longitudinal position (z) by the charge division method. In zero magnetic field the r.m.s. errors measured on a prototype operated in proportional mode are $\sigma(r\phi) \simeq 150\,\mu$m and $\sigma(z) \simeq 5$ cm. We are studying the operation of the tubes in the limited streamer mode, aiming at improving the z-resolution, because of the larger collected charge, without too large a deterioration of the transverse resolution. By using flash ADCs, this device gives the z position in a microsecond, thus providing, in association with similar data from the inner detector, an efficient fast trigger.

The two forward drift chambers are used both for triggering and for improving the end-cap momentum resolution. Each chamber is made of eight planes with a total of 1000 sense wires. The wires are 10 mm apart, and directed along x, y, u, and v. These chambers are based on the design of existing ones, which have space resolutions of 150 μm. For angles smaller than $\sim 20°$ these chambers will take over the track reconstruction.

The combination of the track detectors described above gives, in the 1.2 T field, the momentum resolutions plotted in Fig. 4. The calculation takes into account the thicknesses of the material in the various detectors. The figure shows that the resolution given by the TPC alone is greatly improved by the addition of the inner, outer and forward detectors.

3.4 The RICH counters

The Ring Imaging Cherenkov (RICH) counters are based on the principles outlined in the paper of Séguinot and Ypsilantis [9]: photons in the UV part of the Cherenkov spectrum produce photoelectrons in a drift gas loaded with a chemical substance that absorbs UV light; the photoelectrons are detected and the Cherenkov angle reconstructed. Our detector contains a barrel RICH counter for particles emitted at $90° \pm 50°$ and an end-cap RICH system for detection in the angular range 8°–35°. The parameters of the three detectors are summarized in Table 2.

Table 2

Parameters of the three RICH counters

	Barrel liquid RICH	End-cap liquid RICH	End-cap gas RICH
Radiator	CF_4 (or Ne)	C_6F_{14}	C_4H_{10} (or C_4F_{10})
Angular coverage (°)	40–140	7–40	7–35
Thickness of the radiator (cm)	2.0	1.0	45–65
Total thickness in X_0	0.43	0.17	0.10
Temperature of the radiator (K)	150	300	300
Type of focusing	Proximity	Proximity	Spherical mirror
Depth of the photon detector (cm)	4.0	4.0	4.0
Number of photoelectrons for normal incidence	30	20	10–15
Surface of the detector (m^2)	32	2×7	2×1.75
Max. drift distance (cm)	150	30	20
Number of wires	9000	2×4000	2×5600
Wire pitch (mm)	2.54	5.08	1.27
Number of cathode strips	640	2×300	–

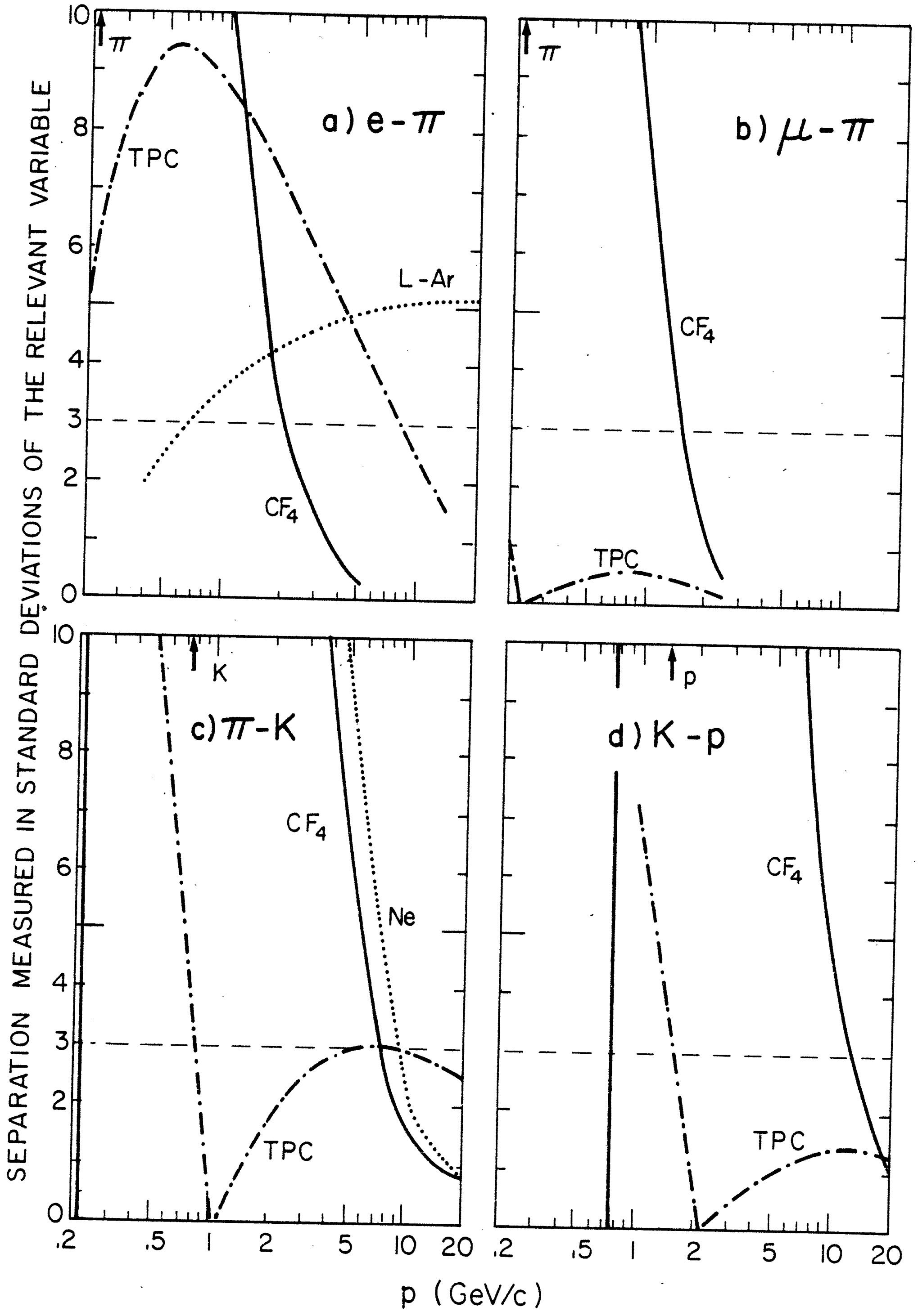

Fig. 5 The separations between pairs of particles produced at $\theta = 90°$ are expressed in standard deviations. For the barrel RICH counter and the $\Delta E/\Delta x$ measurement in the TPC, the quantities plotted on the ordinates are $|\alpha(m_1) - \alpha(m_2)|/\sigma(\alpha)$ and $|E(m_1) - E(m_2)|/\sigma(E)$, respectively, where $\alpha(m_i)$ and $E(m_i)$ are the Cherenkov angle and the average energy deposited by the particle of mass m_i. The dotted line of (a) represents the equivalent number of standard deviations given by the liquid-argon calorimeter. In all the figures the conventional 3 standard deviation separation is indicated by the horizontal dashed line. The arrows indicate thresholds and correspond to a 95% detection efficiency in the cryogenic barrel RICH counter. The vertical lines are thresholds for the lighter particles.

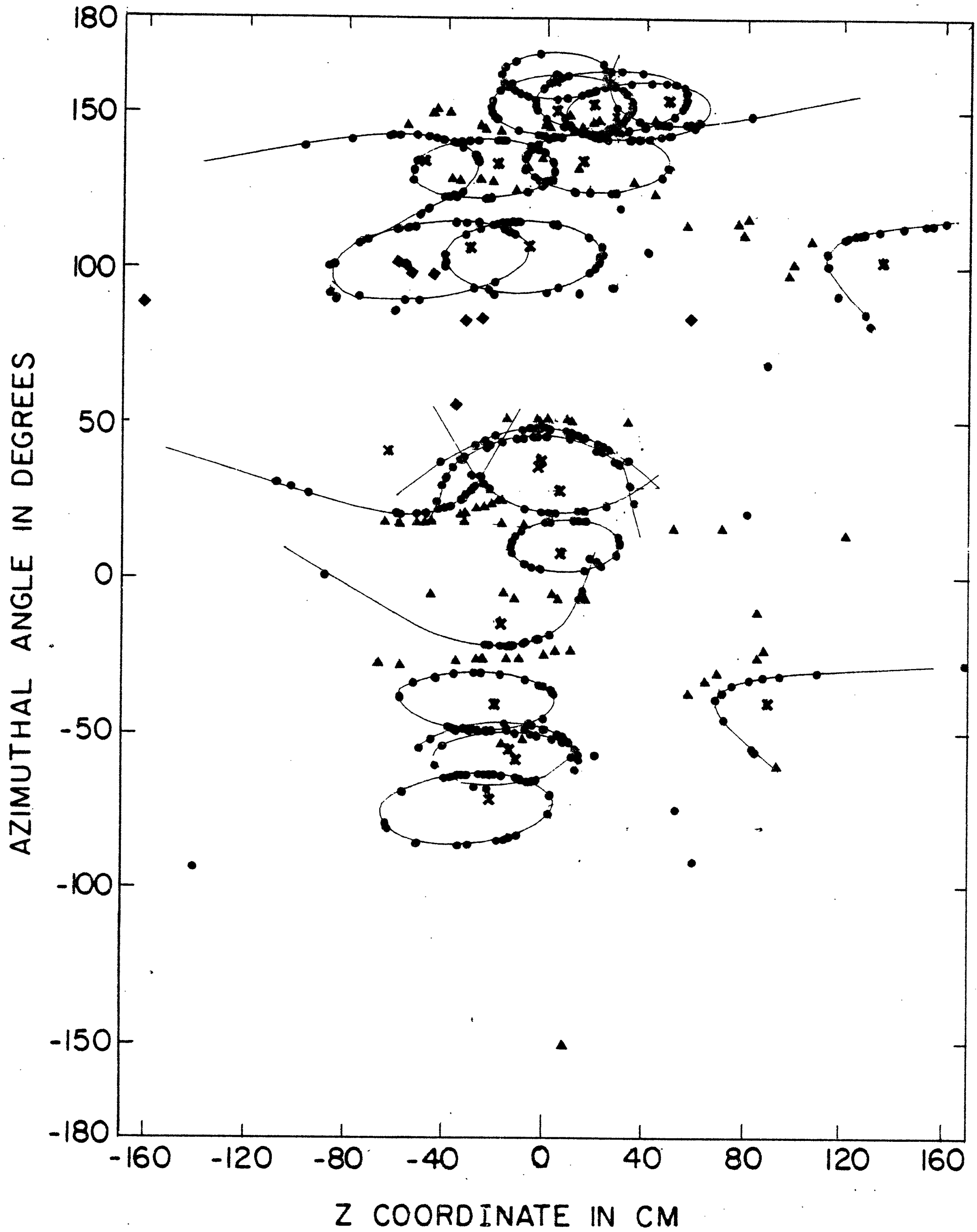

Fig. 6 Monte Carlo simulation of a 90 GeV event (23 charged particles) as seen by the barrel RICH counter. The detector is unfolded so that the abscissa represents the coordinate along the beam axis and the ordinate represents the azimuthal angle. The dots represent detected photons produced in freon, the triangles and diamonds are the impact points of photons radiated in the quartz windows. The crosses are the tracks left directly in the detector by the charged particles. Electrons resulting from photon conversion before the radiator will add a few rings. The lines show the average position of the photons originated in the freon. They are not always closed because, for small polar angle, part of the light is totally reflected inside the liquid.

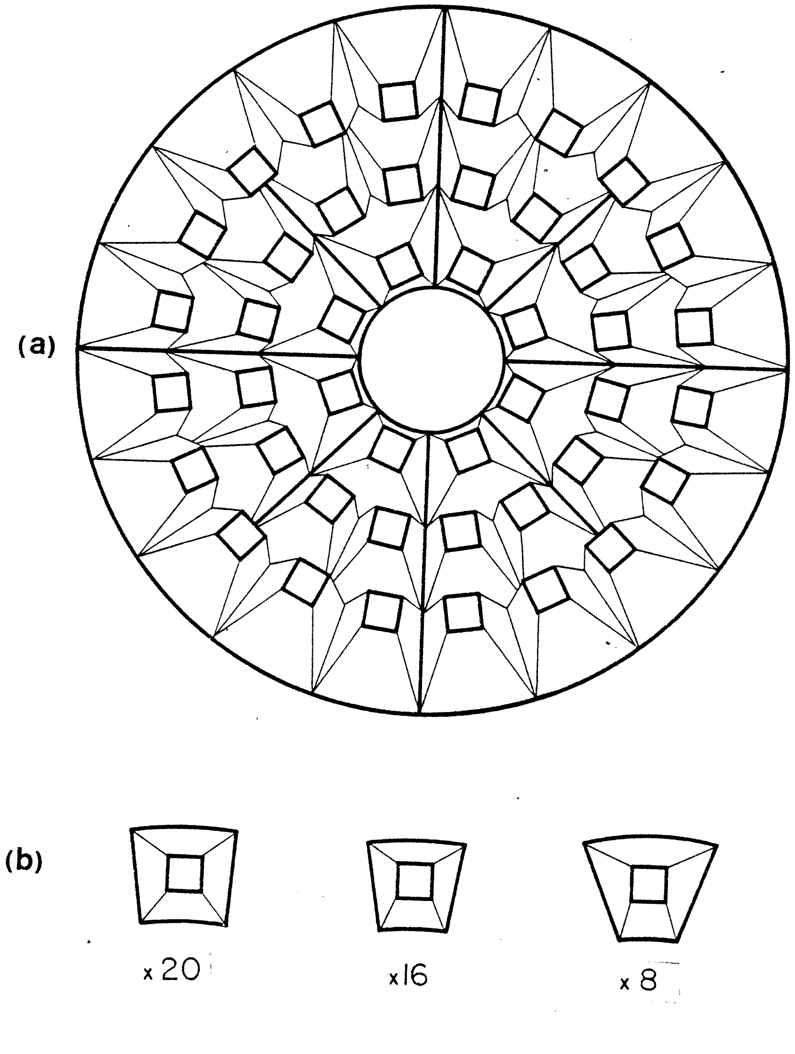

Fig. 7 (a) Perspective view of the 44 cupolas of one of the end-cap RICH counters seen from far away. Only the mirrors and the photon detectors are shown. The lines joining them are drawn to guide the eye. **(b)** The three types of cupolas viewed from the beam-crossing point. The mirrors are different in shape, but the photon detectors are all equal.

The radiator in the barrel RICH is a cylindrical layer of liquefied freon (150 K). The active radiator covers about 90% of the total area, the rest being taken by the quartz frames. Radiator and detector are separated by 30 cm of vacuum; the radiator liquid and the detector gas are each contained in a vessel that is covered by quartz windows (see Fig. 1). The detector is CH_4 gas at room temperature, containing about 1 Torr partial pressure of tetrakis(dimethylamine)ethylene (TMAE), which is a substance photoionized by UV photons (above 5.4 eV). The mean free path for UV photons is about 1 cm. Tests to replace CH_4 with the non-explosive CF_4 are under way. The photoelectrons drift longitudinally, in a 600 V/cm electric field, to a proportional wire detector backed by five cathode strips. The drift time provides the third coordinate.

The expected performance of the barrel liquid counter is such that pions and kaons can be separated in the momentum range from 0.3 to about 8 GeV/c with much more than three standard deviations (see Fig. 5c). Between 8 and $\sim$ 10 GeV/c some additional π/K separation is provided by the $\Delta E/\Delta x$ measurement in the TPC. The possibility of a liquid-neon radiator for the barrel RICH counter is being actively investigated since chromatic aberrations are smaller, so that pions and kaons could be separated up to somewhat higher momentum, as shown in Fig. 5c, although the cryogenic problems would be more complex (temperature: 20 K). Figure 5b shows that in freon, pions and muons are separated up to $\sim$ 1.4 GeV/c, which matches the separation given by the muon chambers for p $\gtrsim$ 2 GeV/c. To study pattern recognition problems, jets have been generated with the Lund model and the charged particle tracks traced through the RICH counter. The resulting Cherenkov photons, together with background photons produced in the quartz, have been analysed and pattern recognized. One event is shown in Fig. 6; the rings are easily reconstructed by the pattern recognition program.

The end-cap regions are covered by two RICH counters mounted in series. One gaseous end-cap counter consists of 44 single counters (cupolas) mounted in three annuli, forming an array similar in structure to a faceted eye (Fig. 7). The cupolas of the three annuli have different lengths (45, 57.5, and 65 cm) to collect more photoelectrons at smaller angles where the effect of the magnetic field on the width of the Cherenkov ring is smaller. Each single counter has an Al-MgF_2-coated spherical mirror of about 1.2 m radius of curvature. We have made beam tests using a prototype counter and isobutane (C_4H_{10}) as radiator, producing rings of 57 mm radius with 12 detected photons. The liquid RICH end-cap counter is similar in principle to the liquid barrel RICH counter. It uses a freon (FC-72), which is liquid at room temperature, as radiator. We have used room-temperature freon liquids in beam tests, observing 20 detected photons per particle with a 1 cm thick radiator. Figure 8 gives the separation in Cherenkov angle between pions, kaons and protons, showing a π/K separation of at least 3 standard deviations in the momentum range 0.3–35 GeV/c. In calculating these curves the smearing of the Cherenkov ring due to the magnetic bending of the particle trajectory has been taken into account.

In the forward direction, the momentum resolution in the solenoidal field deteriorates, as shown in Fig. 4. However, even a poor momentum resolution, combined with the information given by the forward RICH counters, is still sufficient to resolve the particle ambiguity. Once the particle identity is determined, its velocity and thus its momentum can be determined from the radius of the Cherenkov ring, resulting in an improvement of the momentum resolution in the forward direction.

Our test work with RICH counters has so far comprised extensive investigations with gaseous radiators and a 14×18 cm^2 detector, and some measurements with room-temperature liquids. A program of extensive tests is under way on measurements of the transmission and indices of refraction of liquid freons, on the suppression of photoemission from anode wire avalanches caused by the charged particle, and on the reduction of the effects of the longitudinal diffusion when drifting over long distances. An array of end-cap gas counters and a room-temperature liquid radiator counter covering the same area will be constructed and tested in 1982. A prototype neon radiator at 20 K (10 cm in diameter) is now ready and will be tested in February 1982. A full-scale slice of the RICH barrel with a cryogenic radiator has been financed by IN2P3.

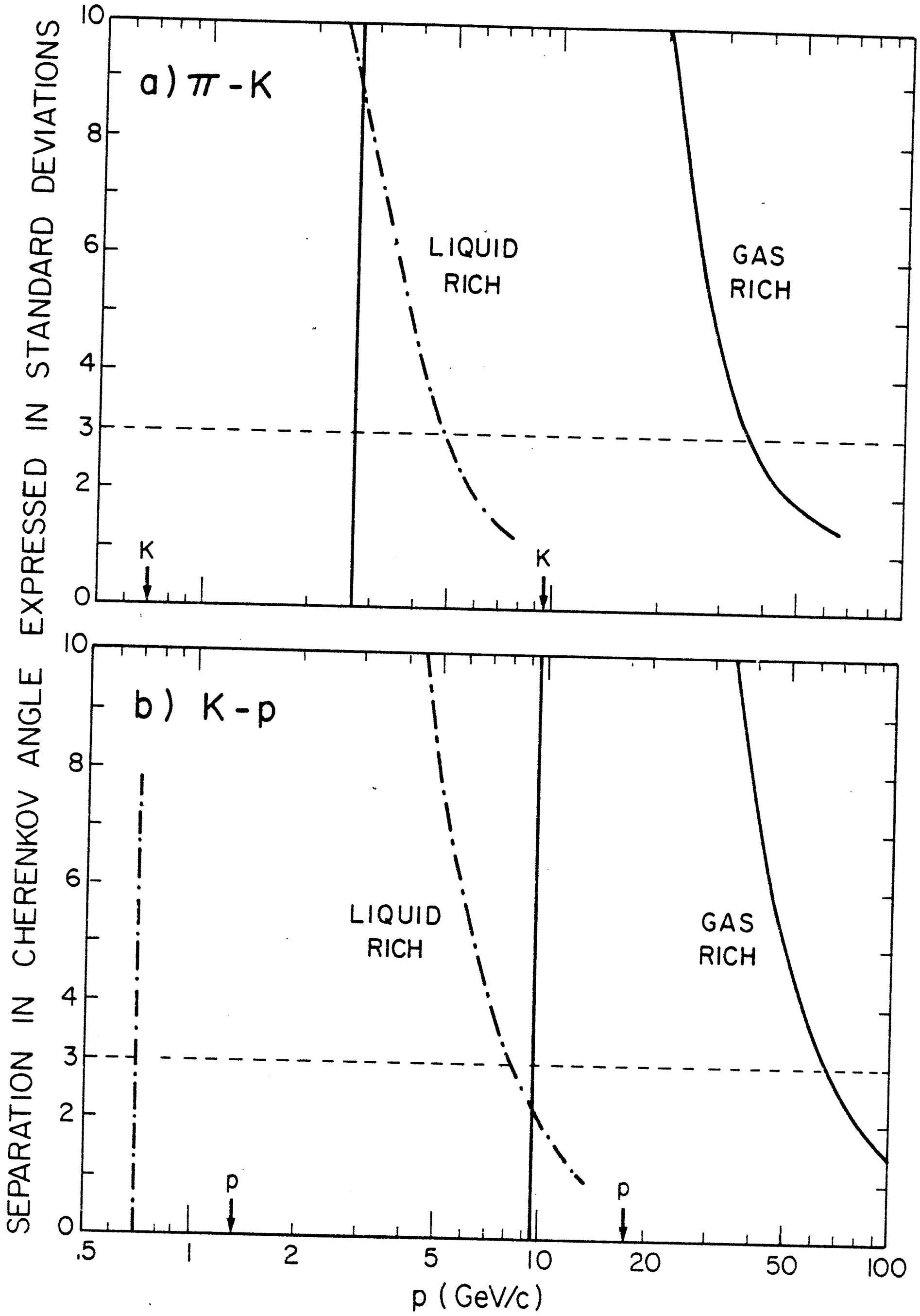

Fig. 8 Pion-kaon and kaon-proton separations given by the forward RICH counters. For both pairs of particles the two counters match, giving many more than the conventional three standard deviation separation in wide momentum ranges: 0.3–35 and 0.7-60 GeV/c, respectively. The thresholds (i.e. the vertical lines) correspond to 95% detection efficiency for the lighter particles. The arrows indicate the threshold for the heavier particles.

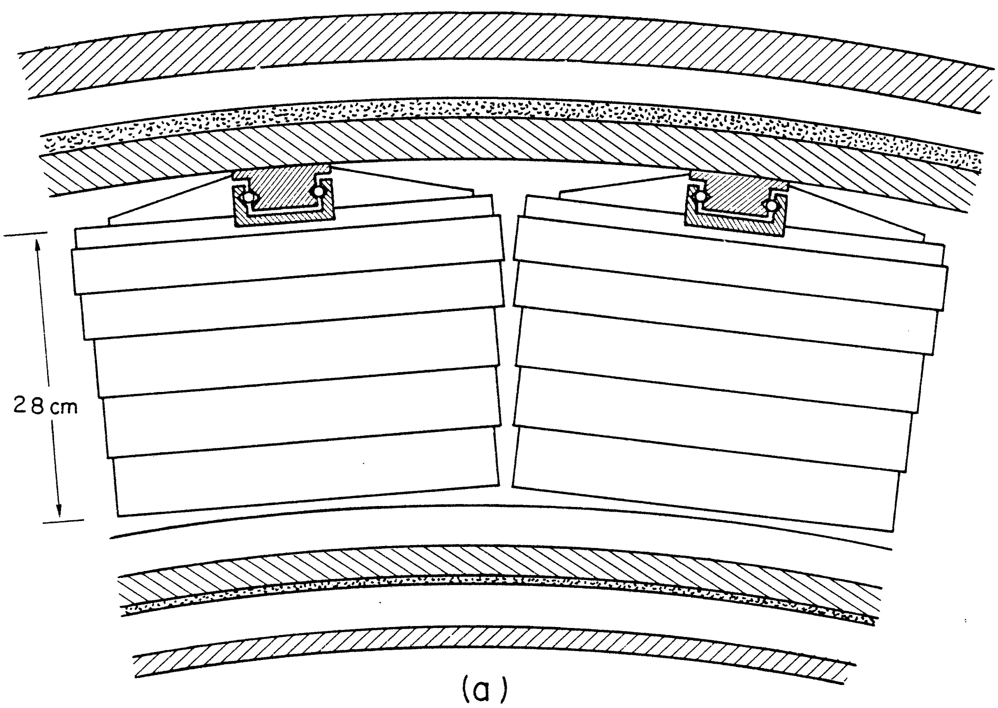

(a)

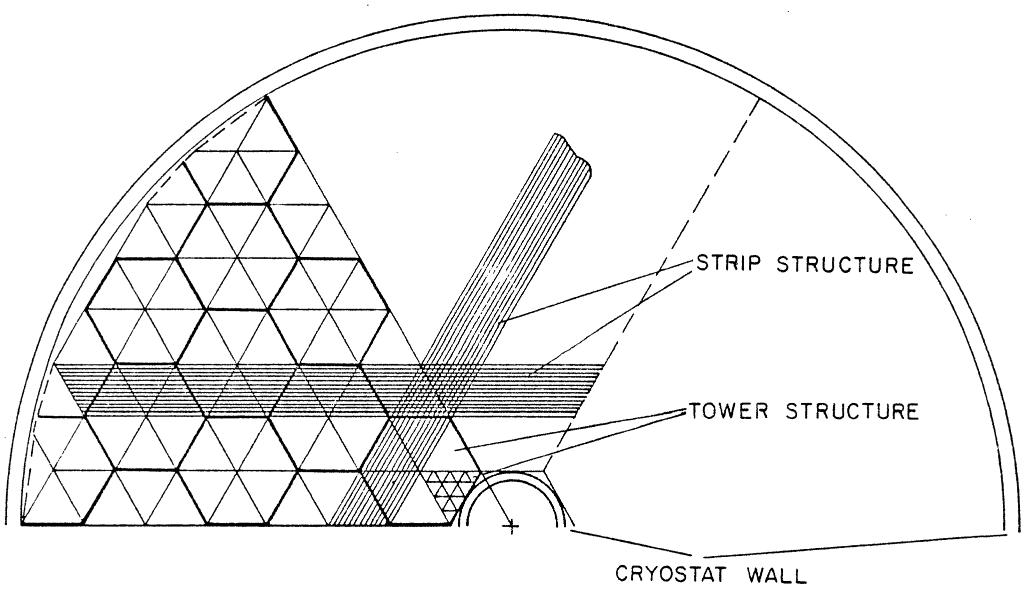

(b)

Fig. 9(a) Cross-section of the cryostat of the barrel liquid-argon calorimeter showing 2 of the 64 modules. **(b)** The tower and strip structure of the forward electromagnetic calorimeter as seen from the centre of the spherical structure. The towers are triangular in shape and grouped together in a hexagonal structure. The corresponding strips in the different towers are electrically connected.

3.5 Electromagnetic calorimeters

As shown in Fig. 1, the lead/liquid-argon electromagnetic calorimeter comprises two forward regions (end-caps) and the central part (barrel). Such a calorimeter is known, from past experience, to be reliable from the point of view of calibration, stability, and operation. The two different portions of the calorimeter have the same capability to resolve electromagnetic showers spatially and longitudinally. The 1 mm thick lead plates (total lead thickness $\sim$ 20.5 X_0) are arranged in a combined strip/tower structure. The readout is subdivided into four longitudinal samples: a) front towers with $2° \times 2°$ granularity; b) three-dimensional strips (1° wide); c) back towers with $4° \times 4°$ granularity, divided into two longitudinal sections. The second section has thicker lead plates (2 mm). This arrangement gives an energy resolution $\Delta E/E \sim A + B/\sqrt{E}$, where in this case A can be kept to $\sim$ 1% because of reliable calibration and easy monitoring. The value of B appearing in the intrinsic resolution is 8.5%. Including the material in front of the calorimeter, it is 13.5% around 1 GeV and 10.5% around 4 GeV.

The barrel section, which fits inside the coil cryostat, is made up of 64 modules, each with a surface of 225×43 cm^2 and a depth of 28 cm (Fig. 9a). These modules are mounted on rails and installed in the same cryostat. This solution minimizes dead spaces and simplifies the cryogenics. The two end-cap calorimeters are made of individual towers of triangular shape which form a hexagonal structure (Fig. 9b) pointing 1 m upstream of the interaction point. The material in front amounts to 0.75 X_0, two-thirds of which are due to the TPC end-plates. The fact that all towers are identical simplifies construction and minimizes costs. Spherical containers are of common use in cryogenic industry. The plates are of smaller size than is needed for 2° granularity. This allows us to go to a 1° granularity at a later stage by adding more electronic channels. The number of channels is calculated, for a first stage, to be 29,000 for the barrel and 10,000 for the two end-caps.

We are also working on a new approach to the barrel electromagnetic calorimeter, which should give a similar energy resolution and better granularity with no cryogenic complications and possibly for a lower price [7]. The High-density Projection Chamber (HPC) aims at three-dimensional imaging of electromagnetic showers with very high granularity in all space coordinates. It consists of four cylindrical, self-supporting, converter structures of the sampling type with 58 samples over 22 X_0 of Pb (Figs. 10a). The charge deposited by the showers will be drifted in sampling slots (Fig. 10b) onto two pick-up proportional chambers. Each chamber will receive charges from two converter structures. The readout is done via cathode pads (Fig. 10c). The granularity along the drift direction is 3 mm or 1.5 mrad. We foresee 12 rows of pads for in-depth sampling along the shower axis. About 4000 pads per chamber will allow for azimuthal granularity of 14 mrad, corresponding to 2.5 cm pad size. Thus the device will present the equivalent of 6×10^6 active cells, each subtending a solid angle of about 2×10^{-5} sr. Within a magnetic field of 1.2 T the HPC is expected to yield an energy resolution of about $12\%/\sqrt{E}$, and good shower separation. Detailed Monte Carlo calculations are under way.

At present a prototype of $15 \times 50 \times 50$ cm^3 is ready to be tested in an electron beam while we are studying various techniques to build the self-supporting cylindrical structures of Fig. 10. By the end of 1982 we shall be in a position to compare this novel calorimeter with the liquid-argon solution presented in Fig. 1 and to choose the solution for the final proposal.

3.6 Hadron calorimeter and muon identifier

The barrel return yoke is made of 38 iron plates, 2.5 cm thick, interleaved with gaps of 1.5 cm; the poles are made of 16 iron plates, 5 cm thick. They will be instrumented as a hadron calorimeter and muon detector. For tracks at 90° this gives a total thickness of 5.5 absorption lengths, to be added to the $\sim$ 1 absorption length of the electromagnetic calorimeter. The gaps are equipped with plastic streamer tubes [10], 1 cm^2 in cross-section, covering a polar region $8° < \theta < 172°$. The number of streamers in the tubes is measured by means of square capacitive pads, electrically connected to form towers pointing to the crossing point. The size of the pads (about 10×10 cm^2) is such as to cover a solid angle of $2° \times 2°$. They are grouped in 4 (3) radial towers in the barrel (end-cap) calorimeter. The total number of towers is $\sim$ 50,000. For the barrel calorimeter the energy resolution will be $0.6/\sqrt{E}$ for single pions of up to about 10 GeV, where longitudinal losses start to be important. The resolution of the forward pole calorimeter will be $0.8/\sqrt{E}$ owing to the coarser sampling; but this is not a limitation in determining the missing transverse momentum caused by the emission of neutrinos, because of the smaller polar angle with respect to the beams.

In the initial phase, 4 gaps of the barrel yoke and 3 gaps of the forward pole will be equipped with streamer tubes with readout on wires and $\pm 45°$ cathode strips (4 cm wide) to provide muon-hadron separation. Monte Carlo calculations show that by making use of the hadron calorimeter towers and of these planes, prompt muons produced inside hadronic jets with energy larger than 2 GeV/c can be identified with 70% efficiency and less than 10% hadron contamination. Later the number of active planes can be increased to reduce further the hadron contamination. External muon chambers are at this moment an open possibility.

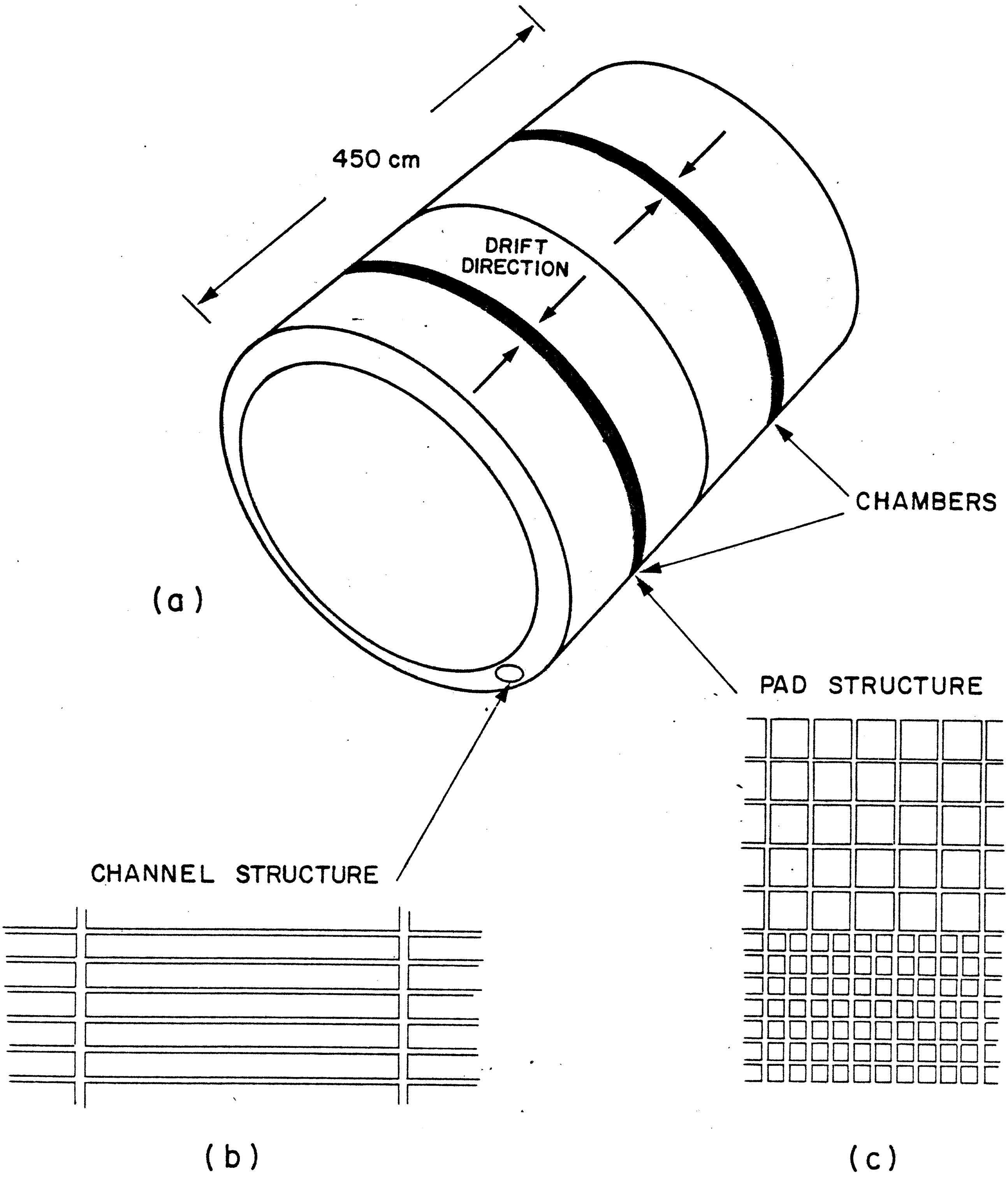

Fig. 10(a) Perspective view of the four cylindrical sectors constituting the high-density projection chamber. The two double annular chambers are also indicated. **(b)** Cross-section of the drift channels. **(c)** Structure of the pads on which the signals of the proportional wires are read. There are 7 + 5 rows of pads in 21 radiation lengths.

3.7 Tagging system

A small-angle tagging system (SAT), covering the angular range 30–100 mrad, is located in front of the low-beta quadrupole. The detector consists of a track chamber followed by 40 lead converters of 5 mm thickness with 10 mm gas sampling. The system uses a readout with pads arranged in concentric circles and has a radial resolution of $\sim$ 3 mm. The energy resolution is $\Delta E/E \simeq 20\%/\sqrt{E}$, which gives on Q^2 a relative error of about 7% in the angular range covered by the SAT. The SAT serves also as an on-line luminosity monitor.

3.8 Vertex detector

At present, high-resolution silicon microstrip detectors are being developed by several members of our collaboration for application in SPS experiments to measure secondary decay vertices of charmed particles. Ion-implanted detectors with a sensitive area of 24×36 mm^2, aluminium strips 20 μm apart, and readout every 60 μm or 120 μm, have recently been tested in a 175 GeV beam at the SPS. A spatial resolution of $\sigma = 10\ \mu$m has been measured using a capacitative charge-division method. Similar strip detectors with some active elements (switches and MOS storage capacitors) on the same chip are now being developed, with the possibility of serial readout. To explore the problems of big-size detectors, chips of 70×70 mm^2 having strips of 15 μm pitch will be tested during this year.

A set-up of three layers of solid-state detectors over a width of 100 mm and a length of 250 mm on the top and bottom of an elliptical beam pipe could be read out using only about 40 lines for each layer. Monte Carlo studies indicate that, with such a set-up, low-multiplicity decays of D mesons could be separated from the primary vertex with an efficiency of around 30% to 50% and a reduction in the combinatorial background by factors from 10 up to a few 1000 in the case of two-body decay and four-body decay, respectively.

3.9 Trigger

The trigger will be a multilevel system; the raw beam crossing rate of $\sim$ 50 kHz will be reduced by a series of event selection criteria prior to data recording. Such a sophistication has been foreseen to take account of uncertainties in background rates at LEP, to be able to trigger efficiently on very simple event topologies, and in an attempt to avoid subsequent data handling problems which could arise from the large number of detector channels.

Fast charged particle triggers will use track counting in the inner and outer detectors, for both the $r\phi$ and z projections. Neutral triggers will use spatially correlated energy sums observed in the electromagnetic and hadronic calorimeters. These two types of triggers, which can be used independently or in conjunction, will operate within a few microseconds of the beam crossing time. We intend, by successively reducing the raw trigger rate, to be able to gate off the ion current in the TPC for a large part of the time, if this proves to be necessary.

A second level of triggering will make use of TPC information and will be made on a time scale of a few beam crossings. Still higher level triggers, which use full detector granularity and involve the processing of digitized time and charge information, will be implemented using programmable processors.

4. COST ESTIMATES

We have been required to "provide, as far as possible, a firm cost estimate for the detector, including its exploitation and a sharing of the costs and responsibilities among the collaborating institutions". At this preliminary stage it is clearly very difficult to comply with all these requests. We have thus proceeded along the following lines.

We have estimated, to the best of our present knowledge, the cost of the mechanical and the electronic components of the detector. The corresponding capital investments appear in the third and fourth columns of Table 3, together with the number of electronics channels of each component. An expert was put in charge of checking the consistency of the cost of all the electronic channels, which according to our definition includes the cost of cables, crates, and power supplies. We have also estimated the manpower (engineers and technicians) necessary to construct the parts which will not be given to outside firms but will be built in the mechanical and electronics workshops of the collaborating institutes. The man-years needed appear in the last column of Table 3. The sums of these estimates give 56.7 MSF and 460 man-years.

Each group has estimated its contributions, integrated over five years (1983–1987), in terms of the foreseen capital investment and of the man-years that his institute will put into building parts of the detector in central workshops, electronics shops, etc. *These estimates are subject to approval by the funding authorities.* The sums of these estimates give 55 MSF of capital money and 550 man-years.

Table 3

Estimates of the capital cost and the manpower needed to build the detector components (1982 prices)

Component	No. of electronics channels	Electronic cost (MSF)	Mechanical cost (MSF)	Total cost (MSF)	Man-years
Magnet system		–	17.0	17.0	40
Inner detector	1 800	0.35	0.4	0.75	20
TPC	20 000	6.0	3.2	9.2	50
Barrel RICH counter	9 600	1.05	4.1	5.15	100
Outer detector	3 100	0.8	0.4	1.2	20
Barrel e.m. calorimeter	29 000	1.5	5.8	7.3	50
Forward e.m. calorimeter	10 000	0.5	2.5[a)]	3.0[a)]	20
Barrel hadron calorimeter	36 500	0.95	1.15	2.1	20
Barrel muon detector	70 000	1.0	0.15	1.15	5
Forward chambers	4 000	0.5	0.8	1.3	20
Forward liquid RICH	8 600	0.85	0.65	1.5	20
Forward gas RICH	11 200	1.1	0.7	1.8	20
End-cap hadronic calorimeter	14 800	0.4	0.6	1.0	15
End-cap muon detector	33 500	0.5	0.1	0.6	5
Small-angle tagger	10 000	0.65	0.2	0.85	5
Trigger system		1.5	–	1.5	10
Microprocessors and computers[b)]		1.5	–	1.5	20
Counting room			0.5	0.5	20
TOTAL	262 100	19.15	37.55[a)]	56.7[a)]	460

a) Cryogenic material for 0.7 MSF is available within the Collaboration; this amount of money has been deducted from the total.
b) Some computers are already available within the Collaboration.

Table 4

Preliminary sharing of responsibilities

Inner detector	Cracow–NIKHEF
TPC	CERN–Collège de France–Lund–Orsay–Saclay–Strasbourg
Barrel RICH counter	Athens–Ecole Polytechnique–Saclay
Outer detector	Paris–Strasbourg
Barrel e.m. calorimeters	Liquid argon: INFN (Bologna–Genoa–Milan–Padua–Rome), HPC: CERN–Bergen–Oxford–Oslo–Rutherford–Stockholm
Hadron calorimeters and muon detectors	CERN
Forward chambers	Wuppertal
Forward liquid RICH	Cracow–NIKHEF
Forward gas RICH	Uppsala–Wuppertal
Forward e.m. calorimeter	Karlsruhe
Small-angle tagger	Bergen–Oslo
Vertex detector	CERN–Saclay–Rutherford

We conclude that, within the uncertainties of the present estimates, the available capital money and manpower approximately balance the needs. During the detailed design of the detector, we aim to fully utilize the available manpower, which appears to exceed the present estimated needs, in order to reduce the capital cost and match the available money. Furthermore some physics groups, with interest in LEP but heavy current commitments, have expressed interest in joining in a full proposal at a later stage. In particular the groups of Valencia and Santander have declared their intention, if funded, to contribute to the hadron calorimeter.

Table 4 gives the preliminary sharing of the responsibilities among the collaborating institutes. The magnet does not appear because it will be financed from the capital investment of all the groups. Its cost corresponds to about one-third of the total available amount of money. Many groups are listed for the barrel electromagnetic calorimeter because of the High-density Projection Chamber, which is under study in parallel with the liquid-argon project. After the final choice of the electromagnetic calorimeter, responsibilities will be rearranged. As far as the solid-state vertex detector is concerned, the cost is still too uncertain for it to appear in Table 3, but the responsible groups are working to have a definite project ready for the proposal.

Acknowledgements

G. Petrucci has greatly contributed to the choices concerning the general structure of the DELPHI detector. We express our appreciation to him, and also to the Technical Service of the CERN EP Division for the preparation of the drawings and to the Editing and Composition Services.

* * *

In the last meeting before submitting this letter of intent the Collaboration has set up a Project Group which, at present, is formed by: U. Amaldi, J.E. Augustin, G. Barbiellini, P. Borgeaud, A.N. Diddens, T. Ekelöf, G. Flügge and G. Kalmus.

REFERENCES AND NOTES

[1] The Berkeley TPC Group has contributed, as observer, to the preparation of the present letter of intent. Members of the group (L. Galtieri, P. Eberhard, D. Nygren and M. Ronan) have participated in meetings of our Collaboration, and members of our Collaboration took part in the data-taking and analysis of the tests quoted in the text.

[2] E. Picasso, Proc. General Meeting on LEP, Villars-sur-Ollon, 1981, ed. M. Bourquin (ECFA 81/54, CERN, Geneva, 1981), p. 32.

[3] J.E. Augustin, Proc. LEP Summer Study, Les Houches, 1978 (CERN 79-01, 1979), Vol. 1, p. 499.

[4] G. Barbiellini et al., The production and detection of Higgs particles at LEP, DESY 79/27 (1979).

[5] G. Barbiellini, B. Richter and J.L. Siegrist, Phys. Lett. **106B** (1981) 414.

[6] The data collected at or near 1 atm are presented in two TPC notes (G. Lynch, TPC resolution studies, TPC-LBL-81-52 and L. Galtieri, N. Hadley and G. Lynch, Preliminary results of the November TPC test, TPC–LBL–82-01) and are discussed in various internal notes of our Collaboration.

[7] G.H. Fischer and O. Ullaland, IEEE Trans. Nucl. Sci. **NS27** (1980) 38.

[8] ANSALDO S.p.A., Genoa, Italy.

[9] J. Séguinot and T. Ypsilantis, Nucl. Instrum. Methods **142** (1977) 377.
T. Ekelöf, J. Séguinot, J. Tocqueville and T. Ypsilantis, Phys. Scripta 23 (1981) 718.

[10] The use of limited streamer tubes in large calorimeters is described in:
G. Battistoni et al., Nucl. Instrum. Methods **176** (1980) 297.
J.E. Augustin et al. (DM2 Collaboration), Phys. Scripta **23** (1981) 623.
M. Jonker et al. (CHARM Collaboration), Phys. Scripta **23** (1981) 677.